Orbital Redistribution in Molecular Nanostructures Mediated by Metal–Organic Bonds

Zechao Yang,[*,†] Martina Corso,[†,⊥] Roberto Robles,[‡,∥] Christian Lotze,[†] Roland Fitzner,[§] Elena Mena-Osteritz,[§] Peter Bäuerle,[§] Katharina J. Franke,[*,†] and Jose I. Pascual[*,†,#]

[†]Institut für Experimentalphysik, Freie Universität Berlin, Arnimallee 14, 14195 Berlin, Germany, [‡]ICN2 - Institut Catala de Nanociencia i Nanotecnologia, Campus UAB, 08193 Bellaterra, Barcelona, Spain, [§]Institut für Organische Chemie II und Neue Materialien, Universität Ulm, Albert-Einstein-Allee 11, 89081 Ulm, Germany, [∥]CSIC - Consejo Superior de Investigaciones Cientificas, ICN2 Building, Campus UAB, 08193 Bellaterra, Barcelona, Spain, [⊥]Centro de Fisica de Materiales CSIC/UPV-EHU, Manuel Lardizabal 5, 20018 San Sebastian, Spain, and Ikerbasque, Basque Foundation for Science, 48011 Bilbao, Spain, and [#]CIC nanoGune, 20018 Donostia-San Sebastian, Spain, and Ikerbasque, Basque Foundation for Science, 48011 Bilbao, Spain

ABSTRACT Dicyanovinyl-quinquethiophene (DCV5T-Me_2) is a prototype conjugated oligomer for highly efficient organic solar cells. This class of oligothiophenes are built up by an electron-rich donor (D) backbone and terminal electron-deficient acceptor (A) moieties. Here, we investigated its structural and electronic properties when it is adsorbed on a Au(111) surface using low temperature scanning tunneling microscopy/spectroscopy (STM/STS) and atomic force microscopy (AFM). We find that DCV5T-Me_2 self-assembles in extended chains, stabilized by intercalated Au atoms. The effect of metal–ligand hybridization with Au adatoms causes an energetic downshift of the DCV5T-Me_2 lowest unoccupied molecular orbital (LUMO) with respect to the uncoordinated molecules on the surface. The asymmetric coordination of a gold atom to only one molecular end group leads to an asymmetric localization of the LUMO and LUMO+1 states at opposite sides. Using model density functional theory (DFT) calculations, we explain such orbital reshaping as a consequence of linear combinations of the original LUMO and LUMO+1 orbitals, mixed by the attachment of a bridging Au adatom. Our study shows that the alignment of molecular orbitals and their distribution within individual molecules can be modified by contacting them to metal atoms in specific sites.

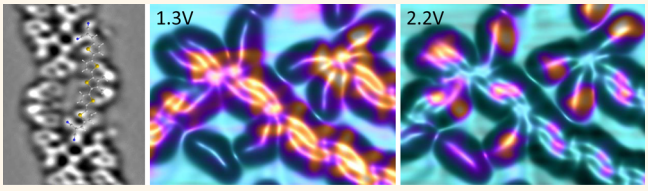

KEYWORDS: oligothiophene · scanning tunneling microscopy · atomic force microscopy · metal–organic coordination · molecular orbital alignment · molecular orbital distribution

The physical and chemical properties of organic thin films are in great part determined by details of their interaction at the interface with a metal support.[1,2] Charge redistribution and orbital realignment can reduce drastically the optical or electronic functionality of the film. Furthermore, hybridization of the metal with reactive molecular groups may enhance vertical charge transfer,[3−6] and induce conformational distortions,[7,8] leading to chemically new molecular species.[9] Even for weak interactions, the metal surface can induce dipolar perturbations to the molecular states.[10−12] The understanding of how molecular levels realign in the proximity of a metal is still under debate.[1,2]

Some organic ligands are very active in bonding to metal adatoms and forming metal–organic nanostructures[13−20] or even meditating the complete reconstruction of the metal surface underneath.[21−25] Due to this strong reactivity, metal adatoms are often captured from the surface and incorporated into the film.[26−29] These adatoms modify the alignment of localized and degenerated orbitals locally and lift their degeneracies by stepwise metal–ligand hybridization.[30,31] Recent works on insulating surfaces tracked precisely the effect of metal atoms on the molecular orbital structure,[32−34] which in many cases induces a renormalization of molecular states that can be described as a simple combination of free-molecule orbitals. Whether this simple picture still applies on a metal–organic interface is still unknown.

Here, we report experimental results that illustrate the crucial role played by gold-adatoms in the assembling and electronic configuration of a functionalized oligothiophene

* Address correspondence to yangzechao@zedat.fu-berlin.de, franke@physik.fu-berlin.de, ji.pascual@nanogune.eu.

Received for review August 8, 2014 and accepted September 22, 2014.

Published online September 22, 2014
10.1021/nn504431e

on a metal surface. We investigate in particular a derivative with an internal acceptor−donor−acceptor architecture, A−D−A oligothiophene DCV5T-Me_2, adsorbed on a Au(111) surface. DCV5T-Me_2 molecules are composed of a central electron-rich quinquethiophenes (5T) backbone with two terminal electron-deficient dicyanovinyl (DCV) groups linked symmetrically, and two methyl (Me_2) substitutions in the central thiophene ring (inset of Figure 1a). The interest in this molecule stems from its potential use as highly efficient photoabsorber in organic photovoltaics: power conversion efficiencies of over 8% have been achieved in vacuum-processed single junction and over 9% in multi-stack bulk heterojunction solar cells.[35,36] The combination of donor and acceptor units in these A−D−A oligothiophenes leads to reduced optical band gaps and excellent photovoltaic properties.[37−45] Their practical use in photovoltaic blends requires efficient charge dynamics, which is favored by the delocalized character of oligothiophene frontier orbitals and by crystal packing. However, the anisotropy of the packing structure,[44] molecular distortions, and the reactivity of the DCV end groups may facilitate the creation of charge traps that inhibit the charge transport.

We find that DCV5T-Me_2 molecules are prone to bond to metal atoms *via* the cyano end groups, and modify, in this way, their free-molecule electronic configuration. The adsorption on a gold substrate at room temperature is dominated by the coordination to gold atoms, which stabilize peculiar bimolecular chain structures. The spectroscopic fingerprint of the metal−ligand bond is an energetic downshift of the lowest unoccupied molecular orbital with respect to the uncoordinated molecule. Interestingly, in molecules bonding to Au adatoms in only one side, scanning tunneling spectroscopy measurements reveal a redistribution of the unoccupied molecular orbitals. The new spatial distribution of the down-shifted LUMO is localized at the coordinated side, while the modified LUMO+1 is localized at the uncoordinated side. Supported by density functional calculations, we rationalize such spatial redistribution of frontier orbitals as a result of the bonding and antibonding combination of the original LUMO and LUMO+1 orbitals. The attachment of one Au atom is found to induce the mixing of the original molecular orbitals into a new set of renormalized orbitals that adapt themselves to the symmetry of the new configuration. Our results thus suggest that the inclusion of metal atoms into the structure of molecular films at specific sites can steer the character of frontier orbitals and, hence, modify the film functionality.

RESULTS AND DISCUSSION

The deposition of submonolayer amounts of DCV5T-Me_2 on Au(111) at room temperature leads to the formation of extended molecular chain structures, and occasional DCV5T-Me_2 monomers dispersed in bare Au(111) regions between them (Figure 1a). The chains are bimolecular linear structures linked by a characteristic motive, differing from the packing structure of bulk.[35] High-resolution STM image (Figure 1b) shows that the linking motive is a bonding node of four molecules pointing their cyano terminations toward each other. Such a bonding configuration is highly unfavorable for the bare electronegative nitrogen terminations, unless a cementing metal atom coordinates to them. Thus, we consider that Au adatoms[46] are trapped and incorporated into the DCV5T-Me_2 chain structures *via* coordination bonds with the cyano moieties of DCV5T-Me_2.[29]

To prove the incorporation of Au atoms and the bonding geometry of the coordinated structure, we measured the molecular nanostructures with noncontact atomic force microscopy (nc-AFM, see Methods

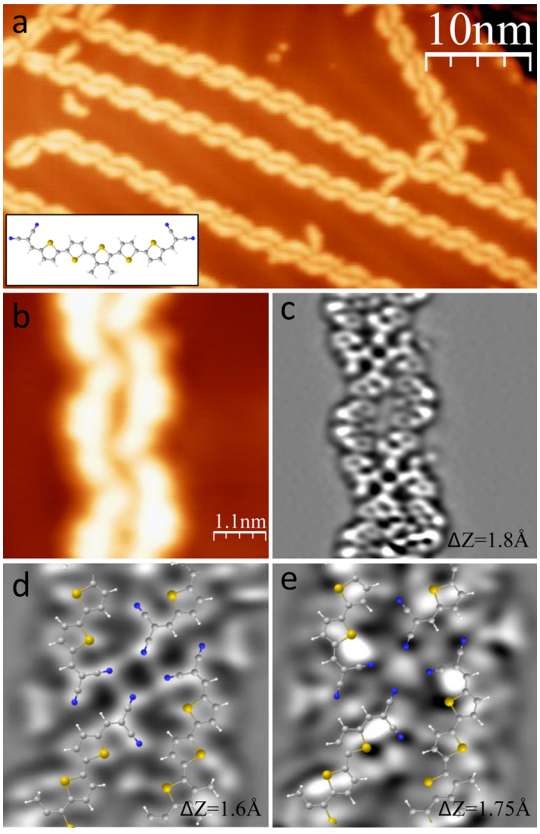

Figure 1. (a) STM image of DCV5T-Me_2 bimolecular chains on Au(111) (I = 18 pA, U = 1.0 V). Inset: chemical structure of the DCV5T-Me_2 molecule (white, hydrogen; gray, carbon; blue, nitrogen; and yellow, sulfur). (b) High-resolution STM image (I = 15 pA, U = 0.1 V) of a chain recorded with a Xe-functionalized tip. (c) Corresponding Laplace filtered nc-AFM image, plotting the amplitude of the frequency shift while scanning at constant tip−sample height. The tip was approached by 1.8 Å toward the sample from an initial position set by the control parameters of I = 15 pA and U = 0.1 V over the molecule. (d and e) Laplace filtered nc-AFM images of the joint of four adjacent molecules around one Au atom. The tip was approached by 1.6 Å (d) and 1.75 Å (e) toward the sample (I = 21 pA, U = 0.11 V) over the molecule, respectively. The size of images in (d) and (e) is 2.45 nm × 2.45 nm.

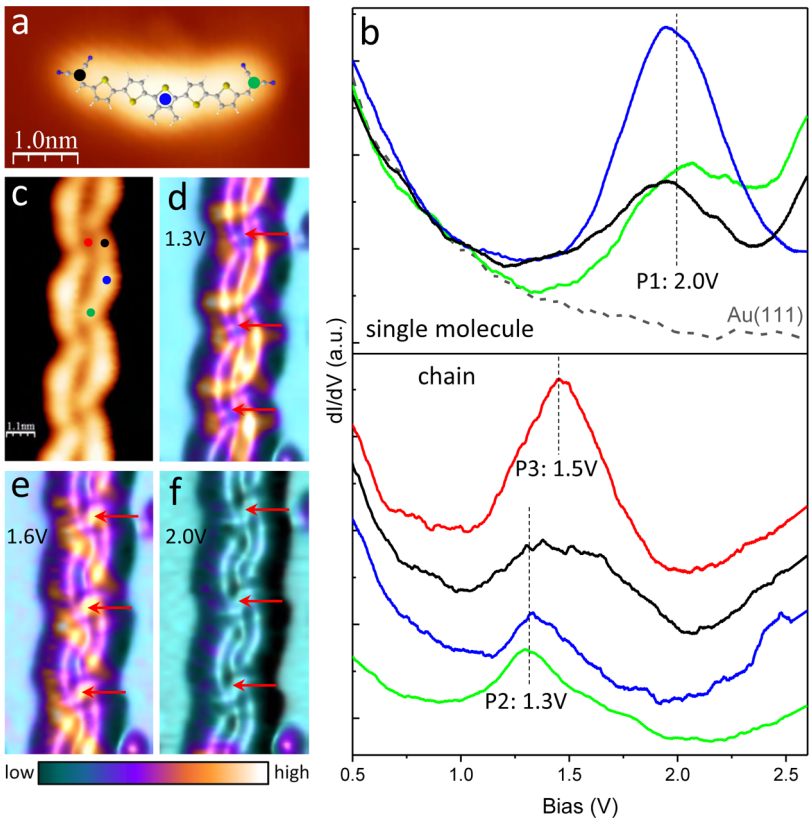

Figure 2. Electronic structure of a single molecule and of a molecule coordinated within a chain. (a) STM image (I = 67 pA, U = 0.89 V) of a single molecule on Au(111), with a DFT optimized configuration superposed. (b) dI/dV spectra acquired with closed feedback at different locations on the single molecule (upper panel, set point, I = 50 pA, U = 0.5 V) and on the molecule within a chain (bottom panel, set point, I = 34 pA, U = 0.2 V), at sites indicated in (a) and (c), respectively. The energetic positions of the resonances in the dI/dV spectra are highlighted by the black dashed vertical lines. Spectra on the coordinated molecule are offset for clarity. (c) STM image (I = 22 pA, U = 0.80 V) of a chain. (d–f) Corresponding dI/dV maps at the energies of the resonances of the coordinated molecules in chains (d), of the Au adatoms (e), and of the single molecule (f), that is, at 1.3, 1.6, and 2.0 V (I = 79 pA), respectively. In (d–f), the dI/dV signals (bright) are overlapped on top of a top-illuminated STM topography. The red arrows indicate the positions of the Au atoms incorporated in the chain.

section). We acquired constant height maps of the shift in resonant frequency (Δf) of a qPlus sensor. The images obtained in the regime of repulsive forces between STM tip and sample reveal the molecular structure of the adsorbed molecule.[47] For these measurements, we functionalized our STM tip with a coadsorbed Xe atom.[48] In this way, it is possible to obtain stable images at close tip-molecule distances, and achieve intramolecular resolution.[47] Figure 1c shows a (Laplace-filtered) nc-AFM image acquired at the same area as the STM image of Figure 1b. The molecular structure can be unambiguously identified from the Δf map. The thiophene backbone appears with the five thiophene rings alternating their orientation, and exposing outward the two central methyl groups. The nc-AFM image also confirms the 4-fold motives formed by four DCV groups around one common point. In spite of the large conformational flexibility of DCV5T-Me_2, most of the molecules appear with this shape. DFT calculations on the free molecule (see Methods section) reveal that, although there are several DCV5T-Me_2 conformers with similar stability in gas phase, the shape observed in nc-AFM images (and sketched in the inset in Figure 1a) corresponds to a global minimum of the free, uncoordinated molecule. This minimum energy configuration has a planar structure, thus enhancing its relative stability when forced to lay in a planar adsorption geometry on a metal surface. Focusing on the linking 4-fold motifs, a rounded protrusion appears between the four cyano groups when imaged at closer tip–sample distances (Figure 1e). This protrusion is unambiguously assigned to the Au atom bridging the four negatively charged cyano groups. Moreover, the four cyano groups are located around the Au adatom following a 4-fold bonding arrangement, supporting that the Au adatom uniformly bonds to the four surrounding molecules (Figure 1d).

To determine the effect of the cementing Au adatoms on the molecular functionality, we studied their electronic configuration by means of STS. As a reference, we measured first spectra on the individual DCV5T-Me_2 monomer, lying on bare gold regions between molecular chains. DCV5T-Me_2 monomers appear in STM images with the same conformation as in the molecular chains (Figure 2a). Differential conductance

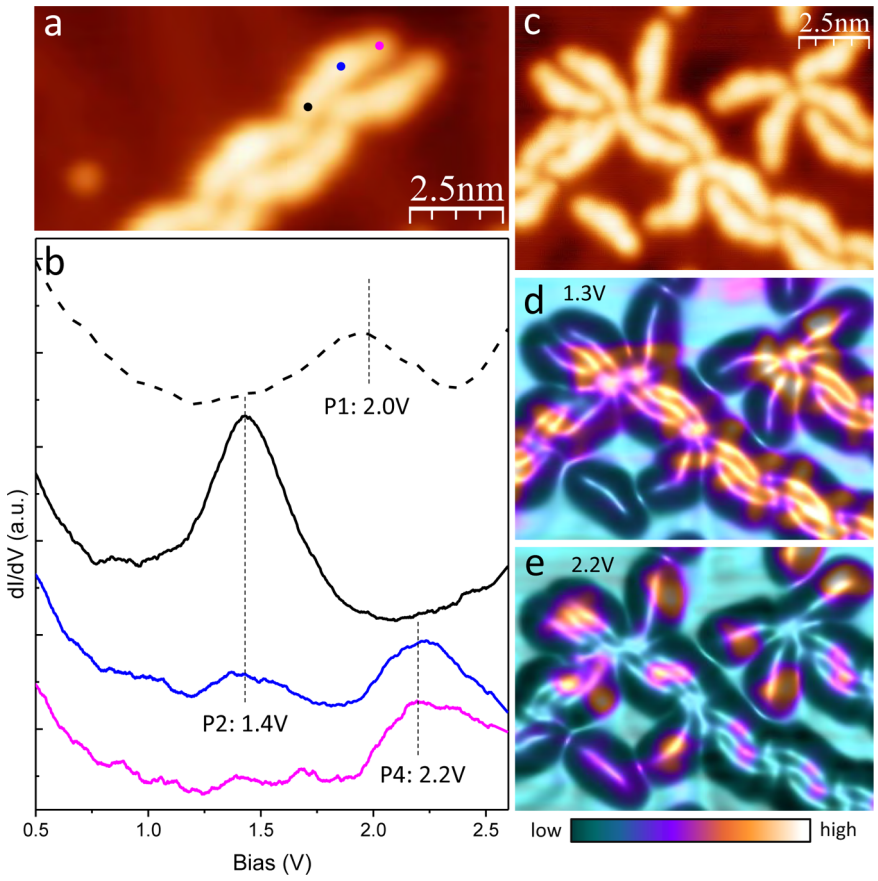

Figure 3. Electronic structure of a one-side-coordinated molecule. (a) STM image (I = 24 pA, U = 0.71 V) of a chain termination showing two molecules without coordination bonds at the end. (b) dI/dV spectra acquired with closed feedback (set point: I = 34 pA, U = 0.2 V) at different locations on the end molecule as indicated in (a). The black dash spectrum taken at one side of the single (uncoordinated) molecule of Figure 2a is shown here as a reference. The energetic positions of the resonances in the dI/dV spectra are highlighted by the black dashed vertical lines, and all the spectra are offset for clarity. (c) STM image (I = 50 pA, U = 0.80 V) of chains with only one-side-coordinated molecules at the ends. (d and e) Corresponding dI/dV maps at the energies of the resonances of the coordinated sides and free sides of the terminal molecules, that is, at 1.3 and 2.2 V (I = 50 pA), respectively. In (d and e), the dI/dV signals (bright) are overlapped on top of a STM topography.

spectra acquired on the center and on the DCV end groups of a DCV5T-Me_2 monomer show a clear peak at 2.0 V (labeled P1 in Figure 2b) with its largest intensity at the center of the molecule, which we assign to the LUMO-derived resonance. The extended character of the LUMO along the whole molecule is in agreement with the free-molecule orbital shape obtained from our DFT calculations (Figure 4b), and confirms that DCV5T-Me_2 monomers maintain to large degree their free-molecule character upon adsorption on the Au(111) surface.

The incorporation of Au atoms modifies the resonance structure of the DCV5T-Me_2 molecules. Lower panel of Figure 2b shows STS spectra recorded on different positions within the chain structures shown in Figure 2c. We find that the new LUMO state is a resonance centered at 1.3 V (P2). This state is observed with larger weight on the sites closer to the Au atoms, as pictured in dI/dV maps (Figure 2d). On top of the Au atom, the state appears centered at 1.5 V (P3) suggesting that this corresponds to an atom-derived localized state.[18] In fact, the dI/dV map recorded at 1.6 V (Figure 2e) allows to resolve the position of individual Au adatoms incorporated in the self-assembled chains, otherwise not visible in the STM topographic images (Figure 2c). The downshift of the LUMO state from 2.0 to 1.3 V, and its localization at the terminal groups, are ascribed to the effect of hybridization with Au adatoms, presumably mixing N lone-pair 2p electrons of cyano groups with Au 6s electron of gold adatoms.[18,29−31,49]

Intercalated metal atoms, therefore, modify the electronic structure of molecular layers, even on weakly interacting substrates. The redistribution and localization of electronic states induced by coordination to Au atoms may affect exciton mobility, whereas, orbital energy shifts modify energy level alignment at the interfaces. However, in real molecular devices, molecules pack in films with geometries different than chain structures reported here, such as molecules asymmetrically bonded to the metal.

To explore the effects of asymmetric bonding to metal atoms, we extend our analysis to molecules at the ends of the molecular chains, as shown in Figure 3. Terminal DCV5T-Me_2 molecules in the chain bond to

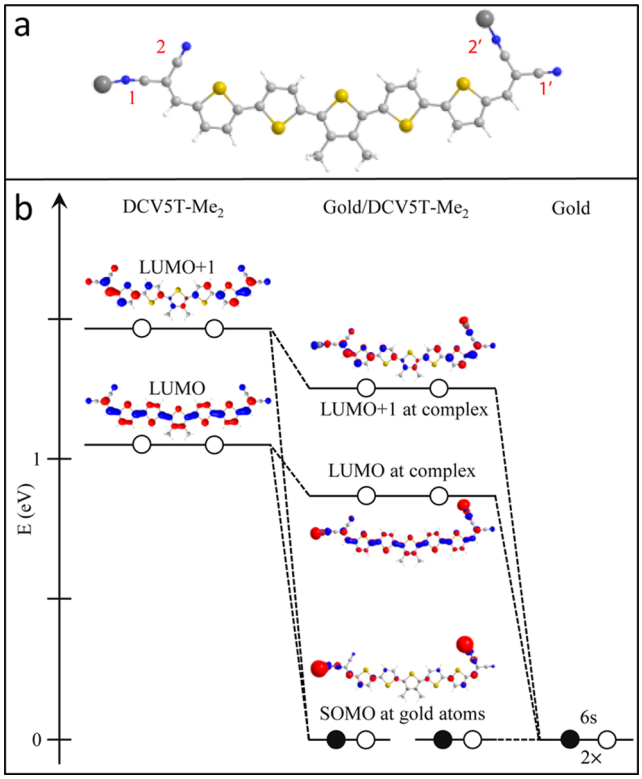

Figure 4. DFT calculations of the Au/DCV5T−Me_2 complex with two Au atoms. (a) The relaxed structure. The gray circles represent Au atoms. The distances between Au atoms and nitrogen atoms from the molecule are 2.2 Å, which are within the range of coordination bond length. (b) Schematic diagram of the calculated energy levels and density of states of the orbitals participating in the formation of the metal−ligand complex. Unoccupied and occupied states are represented by open and filled circles, respectively.

only one Au adatom at one side, while they expose an uncoordinated DCV end group at the other (Figure 3a). The effect of such asymmetric coordination pattern is reflected in the electronic configuration. In Figure 3b, we compare STS spectra taken over both molecular ends. At the coordinated side of the molecule, the first unoccupied resonance appears at 1.4 V similar to the symmetrically coordinated case, whereas the uncoordinated side shows only a higher-lying resonance at 2.2 V (P4). This asymmetric resonance redistribution is reflected in the spatially resolved spectroscopic maps at the corresponding resonance voltages. At 1.3 V, the d*I*/d*V* signal is localized at the joints of cyano groups, corresponding to the position of Au adatoms and coordinated DCV groups (Figure 3d). In contrast, the spectroscopy map at 2.2 V (Figure 3e) shows d*I*/d*V* signal only at the free sides of the terminal molecules. These d*I*/d*V* maps corroborate the fact that the molecular orbital alignment and spatial distribution within individual molecules are strongly modified by metal−ligand coordination.

The origin of the resonance splitting and redistribution cannot simply be explained by a bare orbital shift. As reported in ref 34, coordination to Au atoms enables the mixing of molecular states with gold orbitals. To determine the degree of orbital mixing in these systems, we have carried out DFT calculations of molecular orbitals and charges for (i) an isolated molecule and for a molecule coordinated with (ii) one Au atom and (iii) two Au atoms. Due to the weak interaction of the supporting Au(111) substrate with the DCV5T-Me_2 molecule[12] and the negligible spatial overlap between adjacent molecules, these results reproduce the main trends observed in our experiments. DCV5T-Me_2 has four nonequivalent cyano groups, which are labeled as 1, 1′, 2, and 2′ in Figure 4a. To simulate the experimentally determined bonding structure, we calculated a metal−organic complex with two Au atoms bonded at sites 1 and 2′. The energy optimized structure reproduces a CN−Au bond length of 2.2 Å, which is characteristic for coordination bonds.[13] Similarly, the complex with only one Au atom (located at site 2′, Figure 5a) possesses a coordination bond with bond length of 2.3 Å. Hence, our simulations reproduce the chemical activity of CN end groups to form a local bond with gold atoms.

We look first into the effect of the metal−organic bond on the orbital structure of the complex with two Au atoms. Figure 4b presents the calculated energy levels and spatial distribution of atomic and molecular orbitals around the chemical potential. The LUMO and LUMO+1 of the isolated molecule interact with the 6s states of the gold atoms, resulting in a set of new orbitals (central column of Figure 4b). The states with the lowest energy are two singly occupied orbitals (SOMO) localized at the gold atoms (regarded as the zero point of the system) and mainly with Au(6s)

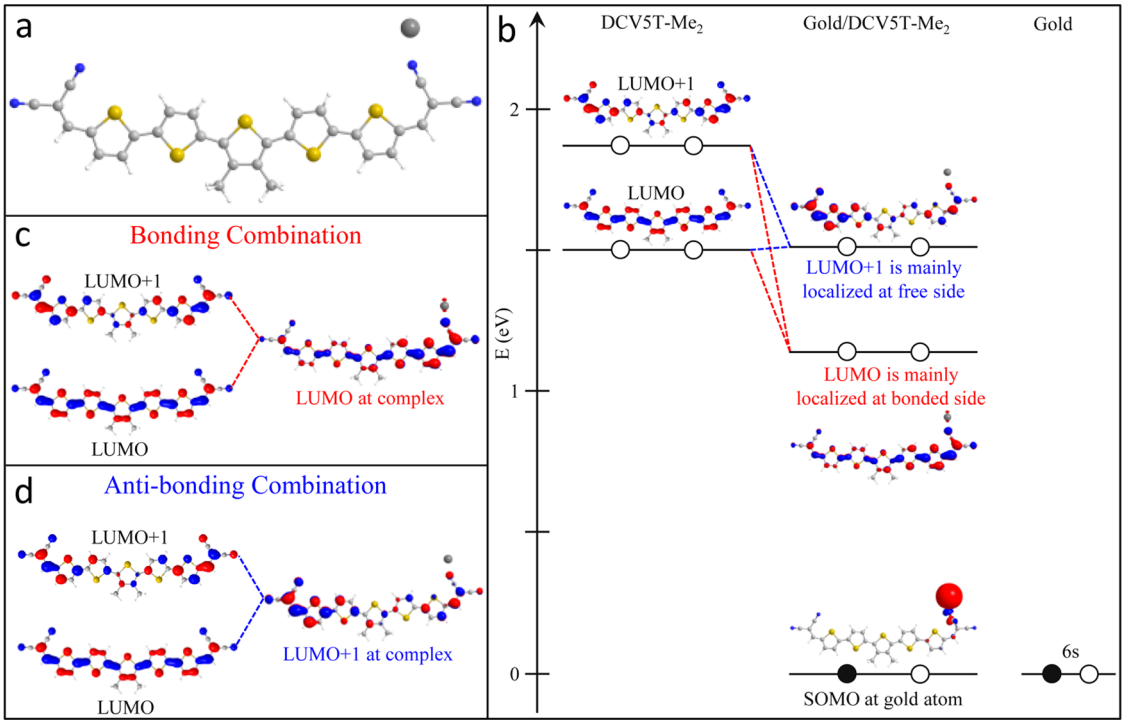

Figure 5. DFT calculations of the Au/DCV5T-Me$_2$ complex with one Au atom. (a) The relaxed structure. The gray circle represents the Au atom. The distance between Au atom and nitrogen atom from the molecule is 2.3 Å. (b) Schematic diagram of the calculated energy levels and density of states of the orbitals participating in the formation of the metal−ligand complex. Unoccupied and occupied states are represented by open and filled circles, respectively. (c and d) The new LUMO and LUMO+1 orbitals with asymmetric shape at the complex originate from the bonding combination and antibonding combination of the original LUMO and LUMO+1 orbitals of the molecule, respectively.

character. Above them, other states exhibit the symmetry and characteristic nodal structures of LUMO and LUMO+1 orbitals of the isolated molecule, with a down-shifted energy alignment. The coordination bond with the gold atoms is weak, amounting to 284 meV. A Mulliken analysis of the charge distribution shows no significant charge transfer between the Au atoms and the molecule, but just some charge redistribution within the molecules.

For the case of bonding to only one single Au atom, the simulations reproduce the asymmetric spatial distribution of the molecular states. Figure 5b shows the calculated energy levels and orbital amplitude isosurfaces for the complex with only one Au atom bonding to the 2′ site. Three new orbitals are generated at the metal−molecule complex from the two original orbitals at the molecule and the Au(6s) state (central column of Figure 5b). The SOMO state near the zero point energy is localized at the Au−N node. We also find here no significant charge transfer between the Au atom and the molecules, and an overall energy down shift of the renormalized LUMO and LUMO+1 states, in consistency with the experimental case. However, now the states show a clear asymmetry in the orbital shape: the new LUMO appears localized around the molecular end contacting with Au atom, whereas the new LUMO+1 state shows larger intensity at the opposite side of the metal−ligand bond.

We note that for the free, uncoordinated molecule, the LUMO is mirror symmetric with respect to the center of the molecule, whereas the LUMO+1 is antisymmetric (Figure 5c,d). Hence, the renormalized molecular states necessarily involve the mixture of free-molecule states to adapt themselves to the new geometry. This can be interpreted at the very basic level as a linear combination of free molecular orbitals. In fact, our DFT results show that the Au(6s) states mix with only the LUMO and LUMO+1 orbitals of the free molecule giving rise to a new set of states with a spatial distribution adopting the symmetry of the singly coordinated molecule. The molecular and atomic occupied states, in contrast, remain fairly unperturbed. Comparing the orbital shapes from Figure 4b, the splitting of the original LUMO into two asymmetric states is then described by the respective addition and subtraction of some weight of the original LUMO+1 to (Figure 5c) and from (Figure 5d) the free LUMO.

CONCLUSIONS

In summary, we have shown that A−D−A oligothiophene DCV5T-Me$_2$ self-assembles on a Au(111) surface *via* the capture and coordination to Au adatoms, mediating the formation of metal−organic chains. The coordination with the metal proceeds *via* terminal CN groups and causes a characteristic energy downshift of the LUMO-derived state with respect

to uncoordinated single molecules. Interestingly, we observe that for molecules showing coordination to Au adatoms in only one of the two ends, the down-shifted LUMO appears localized at the coordinated side with the new LUMO+1 localized at the opposite side. We interpreted this new set of states using a linear combination of molecular orbitals, in which the Au atom triggers a mixing of unoccupied states to produce a new set of orbitals that are adapted to the new bonding geometry. This depicts a tuning strategy to manipulate the orbital character of molecular films by the inclusion of intercalated metal atoms in their structure.

METHODS

Our experiments were performed in a combined STM/AFM at a temperature of 5 K and under ultrahigh vacuum conditions. Nc-AFM measurements were carried out using qPlus tuning fork design,[50] operated in frequency modulation mode with subangstrom oscillation amplitudes. The Au(111) surface was cleaned by repeated cycles of Ne^+ sputtering and subsequent annealing to 750 K. DCV5T-Me_2 molecules were evaporated on the sample kept at room temperature from an organic molecular evaporator with a quartz balance for controlling the deposition coverage. All the STM topographic images were acquired in constant current mode with typical parameters of 20−120 pA and 0.5−1.4 V, whereas AFM images were acquired by mapping the frequency-shift (Δf) of the qPlus sensor in constant height mode. To increase the resolution in AFM images, the STM tip was functionalized with Xe atoms co-deposited on the surface. The d*I*/d*V* spectra and maps were recorded with a lock-in amplifier with typical modulation amplitude of 12 mV and frequency of 740 Hz. The topographic data were processed with Nanotec WSxM software[51] and the spectra data were processed with Mike Ruby's Spectroscopy Manager.[52]

DFT calculations were performed using the GAUSSIAN 03W program package.[53] All calculations including geometry optimizations and electronic excitation energies were carried out on isolated molecular assemblies using the B3LYP exchange-correlation functional. The 6-31G and LanL2DZ basis sets were chosen for single molecule and Au/molecule systems, respectively, as a compromise between accuracy and applicability to large molecules and metal atoms.

Conflict of Interest: The authors declare no competing financial interest.

Acknowledgment. Z.Y. acknowledges the Chinese CSC program for his grant. M.C. acknowledges the Alexander von Humboldt Foundation for financial support. Funding by the DFG (Sfb 658 and Grant No. FR2726/1) as well as the Focus Area "Functional Materials at the Nanoscale" of the Freie Universität Berlin is gratefully acknowledged. We also acknowledge financial support from Spanish MINECO (Grants No. MAT2012-38318-C03-02 and MAT2013-46593-C6-01).

REFERENCES AND NOTES

1. Ishii, H.; Sugiyama, K.; Ito, E.; Seki, K. Energy Level Alignment and Interfacial Electronic Structures at Organic/Metal and Organic/Organic Interfaces. *Adv. Mater.* **1999**, *11*, 605–625.
2. Cahen, D.; Kahn, A. Electron Energetics at Surfaces and Interfaces: Concepts and Experiments. *Adv. Mater.* **2003**, *15*, 271–277.
3. Lu, X.; Grobis, M.; Khoo, K. H.; Louie, S. G.; Crommie, M. F. Spatially Mapping the Spectral Density of a Single C_{60} Molecule. *Phys. Rev. Lett.* **2003**, *90*, 096802.
4. Lu, X.; Grobis, M.; Khoo, K. H.; Louie, S. G.; Crommie, M. F. Charge Transfer and Screening in Individual C_{60} Molecules on Metal Substrates: A Scanning Tunneling Spectroscopy and Theoretical Study. *Phys. Rev. B* **2004**, *70*, 115418.
5. Fernandez-Torrente, I.; Monturet, S.; Franke, K. J.; Fraxedas, J.; Lorente, N.; Pascual, J. I. Long-Range Repulsive Interaction between Molecules on a Metal Surface Induced by Charge Transfer. *Phys. Rev. Lett.* **2007**, *99*, 176103.
6. Henningsen, N.; Rurali, R.; Franke, K.; Fernández-Torrente, I.; Pascual, J. Trans to Cis Isomerization of an Azobenzene Derivative on aCu(100) Surface. *Appl. Phys. A: Mater. Sci. Process.* **2008**, *93*, 241–246.
7. Wegner, D.; Yamachika, R.; Wang, Y.; Brar, V. W.; Bartlett, B. M.; Long, J. R.; Crommie, M. F. Single-Molecule Charge Transfer and Bonding at an Organic/Inorganic Interface: Tetracyanoethylene on Noble Metals. *Nano Lett.* **2008**, *8*, 131–135.
8. Harutyunyan, H.; Callsen, M.; Allmers, T.; Caciuc, V.; Blugel, S.; Atodiresei, N.; Wegner, D. Hybridisation at the Organic-Metal Interface: A Surface-Scientific Analogue of Huckel's Rule? *Chem. Commun.* **2013**, *49*, 5993–5995.
9. Heimel, G.; Duhm, S.; Salzmann, I.; Gerlach, A.; Strozecka, A.; Niederhausen, J.; Bürker, C.; Hosokai, T.; Fernandez-Torrente, I.; Schulze, G.; *et al.* Charged and Metallic Molecular Monolayers through Surface-Induced Aromatic Stabilisation. *Nat. Chem.* **2013**, *5*, 187–194.
10. Qiu, X. H.; Nazin, G. V.; Ho, W. Vibronic States in Single Molecule Electron Transport. *Phys. Rev. Lett.* **2004**, *92*, 206102.
11. Fernández-Torrente, I.; Franke, K. J.; Pascual, J. I. Structure and Electronic Configuration of Tetracyanoquinodimethane Layers on a Au(111) Surface. *Int. J. Mass. Spect.* **2008**, *277*, 269–273.
12. Varene, E.; Pennec, Y.; Tegeder, P. Assembly and Electronic Structure of Octithiophene on Au(111). *Chem. Phys. Lett.* **2011**, *515*, 141–145.
13. Barth, J. V. Molecular Architectonic on Metal Surfaces. *Annu. Rev. Phys. Chem.* **2007**, *58*, 375–407.
14. Cicoira, F.; Santato, C.; Rosei, F. Two-Dimensional Nanotemplates as Surface Cues for the Controlled Assembly of Organic Molecules. *Top. Curr. Chem.* **2008**, *285*, 203–267.
15. Liang, H.; He, Y.; Ye, Y.; Xu, X.; Cheng, F.; Sun, W.; Shao, X.; Wang, Y.; Li, J.; Wu, K. Two-dimensional Molecular Porous Networks Constructed by Surface Assembling. *Coord. Chem. Rev.* **2009**, *253*, 2959–2979.
16. Stepanow, S.; Lin, N.; Payer, D.; Schlickum, U.; Klappenberger, F.; Zoppellaro, G.; Ruben, M.; Brune, H.; Barth, J.; Kern, K. Surface-Assisted Assembly of 2D Metal-Organic Networks That Exhibit Unusual Threefold Coordination Symmetry. *Angew. Chem., Int. Ed.* **2007**, *46*, 710–713.
17. Schlickum, U.; Decker, R.; Klappenberger, F.; Zoppellaro, G.; Klyatskaya, S.; Ruben, M.; Silanes, I.; Arnau, A.; Kern, K.; Brune, H.; *et al.* Metal-Organic Honeycomb Nanomeshes with Tunable Cavity Size. *Nano Lett.* **2007**, *7*, 3813–3817.
18. Henningsen, N.; Rurali, R.; Limbach, C.; Drost, R.; Pascual, J. I.; Franke, K. J. Site-Dependent Coordination Bonding in Self-Assembled Metal-Organic Networks. *J. Phys. Chem. Lett.* **2011**, *2*, 55–61.
19. Tseng, T.-C.; Abdurakhmanova, N.; Stepanow, S.; Kern, K. Hierarchical Assembly and Reticulation of Two-Dimensional Mn- and Ni-$TCNQ_x$ (x = 1, 2, 4) Coordination Structures on a Metal Surface. *J. Phys. Chem. C* **2011**, *115*, 10211–10217.
20. Liu, J.; Lin, T.; Shi, Z.; Xia, F.; Dong, L.; Liu, P. N.; Lin, N. Structural Transformation of Two-Dimensional Metal-Organic Coordination Networks Driven by Intrinsic In-Plane Compression. *J. Am. Chem. Soc.* **2011**, *133*, 18760–18766.
21. Maksymovych, P.; Sorescu, D. C.; Yates, J. T. Gold-Adatom-Mediated Bonding in Self-Assembled Short-Chain Alkanethiolate Species on the Au(111) Surface. *Phys. Rev. Lett.* **2006**, *97*, 146103.

22. Driver, S. M.; Zhang, T.; King, D. A. Massively Cooperative Adsorbate-Induced Surface Restructuring and Nanocluster Formation. *Angew. Chem., Int. Ed.* **2007**, *46*, 700–703.
23. Maksymovych, P.; Yates, J. T. Au Adatoms in Self-Assembly of Benzenethiol on the Au(111) Surface. *J. Am. Chem. Soc.* **2008**, *130*, 7518–7519.
24. Rossel, F.; Brodard, P.; Patthey, F.; Richardson, N. V.; Schneider, W.-D. Modified Herringbone Reconstruction on Au(111) Induced by Self-assembled Azure A Islands. *Surf. Sci.* **2008**, *602*, L115–L117.
25. Sun, J. T.; Gao, L.; He, X. B.; Cheng, Z. H.; Deng, Z. T.; Lin, X.; Hu, H.; Du, S. X.; Liu, F.; Gao, H.-J. Surface Reconstruction Transition of Metals Induced by Molecular Adsorption. *Phys. Rev. B* **2011**, *83*, 115419.
26. Pawin, G.; Wong, K.; Kim, D.; Sun, D.; Bartels, L.; Hong, S.; Rahman, T.; Carp, R.; Marsella, M. A Surface Coordination Network Based on Substrate-Derived Metal Adatoms with Local Charge Excess. *Angew. Chem., Int. Ed.* **2008**, *47*, 8442–8445.
27. Shi, Z.; Lin, N. Porphyrin-Based Two-Dimensional Coordination Kagome Lattice Self-Assembled on a Au(111) Surface. *J. Am. Chem. Soc.* **2009**, *131*, 5376–5377.
28. Björk, J.; Matena, M.; Dyer, M. S.; Enache, M.; Lobo-Checa, J.; Gade, L. H.; Jung, T. A.; Stöhr, M.; Persson, M. STM Fingerprint of Molecule-Adatom Interactions in a Self-Assembled Metal-Organic Surface Coordination Network on Cu(111). *Phys. Chem. Chem. Phys.* **2010**, *12*, 8815–8821.
29. Faraggi, M. N.; Jiang, N.; Gonzalez-Lakunza, N.; Langner, A.; Stepanow, S.; Kern, K.; Arnau, A. Bonding and Charge Transfer in Metal-Organic Coordination Networks on Au(111) with Strong Acceptor Molecules. *J. Phys. Chem. C* **2012**, *116*, 24558–24565.
30. Nazin, G. V.; Qiu, X. H.; Ho, W. Visualization and Spectroscopy of a Metal-Molecule-Metal Bridge. *Science* **2003**, *302*, 77–81.
31. Wang, W.; Shi, X.; Lin, C.; Zhang, R. Q.; Minot, C.; Van Hove, M. A.; Hong, Y.; Tang, B. Z.; Lin, N. Manipulating Localized Molecular Orbitals by Single-Atom Contacts. *Phys. Rev. Lett.* **2010**, *105*, 126801.
32. Repp, J.; Meyer, G.; Paavilainen, S.; Olsson, F. E.; Persson, M. Imaging Bond Formation Between a Gold Atom and Pentacene on an Insulating Surface. *Science* **2006**, *312*, 1196–1199.
33. Liljeroth, P.; Swart, I.; Paavilainen, S.; Repp, J.; Meyer, G. Single-Molecule Synthesis and Characterization of Metal-Ligand Complexes by Low-Temperature STM. *Nano Lett.* **2010**, *10*, 2475–2479.
34. Albrecht, F.; Neu, M.; Quest, C.; Swart, I.; Repp, J. Formation and Characterization of a Molecule-Metal-Molecule Bridge in Real Space. *J. Am. Chem. Soc.* **2013**, *135*, 9200–9203.
35. Fitzner, R.; Mena-Osteritz, E.; Mishra, A.; Schulz, G.; Reinold, E.; Weil, M.; Körner, C.; Ziehlke, H.; Elschner, C.; Leo, K.; *et al.* Correlation of π-Conjugated Oligomer Structure with Film Morphology and Organic Solar Cell Performance. *J. Am. Chem. Soc.* **2012**, *134*, 11064–11067.
36. Meerheim, R.; Körner, C.; Leo, K. Highly efficient organic multi-junction solar cells with a thiophene based donor material. *Appl. Phys. Lett.* **2014**, *105*, 063306.
37. Schulze, K.; Uhrich, C.; Schüppel, R.; Leo, K.; Pfeiffer, M.; Brier, E.; Reinold, E.; Bäuerle, P. Efficient Vacuum-Deposited Organic Solar Cells Based on a New Low-Bandgap Oligothiophene and Fullerene C_{60}. *Adv. Mater.* **2006**, *18*, 2872–2875.
38. Schueppel, R.; Schmidt, K.; Uhrich, C.; Schulze, K.; Wynands, D.; Brédas, J. L.; Brier, E.; Reinold, E.; Bu, H.-B.; Baeuerle, P.; *et al.* Optimizing Organic Photovoltaics Using Tailored Heterojunctions: A Photoinduced Absorption Study of Oligothiophenes with Low Band Gaps. *Phys. Rev. B* **2008**, *77*, 085311.
39. Wynands, D.; Levichkova, M.; Riede, M.; Pfeiffer, M.; Baeuerle, P.; Rentenberger, R.; Denner, P.; Leo, K. Correlation between Morphology and Performance of Low Bandgap Oligothiophene: C_{60} Mixed Heterojunctions in Organic Solar Cells. *J. Appl. Phys.* **2010**, *107*, 014517.
40. Mishra, A.; Uhrich, C.; Reinold, E.; Pfeiffer, M.; Bäuerle, P. Synthesis and Characterization of Acceptor-Substituted Oligothiophenes for Solar Cell Applications. *Adv. Energy Mater.* **2011**, *1*, 265–273.
41. Fitzner, R.; Reinold, E.; Mishra, A.; Mena-Osteritz, E.; Ziehlke, H.; Körner, C.; Leo, K.; Riede, M.; Weil, M.; Tsaryova, O. *et al.* Dicyanovinyl-Substituted Oligothiophenes: Structure-Property Relationships and Application in Vacuum-Processed Small Molecule Organic Solar Cells. *Adv. Funct. Mater.* **2011**, *21*, 897–910.
42. Haid, S.; Mishra, A.; Uhrich, C.; Pfeiffer, M.; Bäuerle, P. Dicyanovinylene-Substituted Selenophene-Thiophene Co-oligomers for Small-Molecule Organic Solar Cells. *Chem. Mater.* **2011**, *23*, 4435–4444.
43. Mishra, A.; Bäuerle, P. Small Molecule Organic Semiconductors on the Move: Promises for Future Solar Energy Technology. *Angew. Chem., Int. Ed.* **2012**, *51*, 2020–2067.
44. Schrader, M.; Fitzner, R.; Hein, M.; Elschner, C.; Baumeier, B.; Leo, K.; Riede, M.; Bäuerle, P.; Andrienko, D. Comparative Study of Microscopic Charge Dynamics in Crystalline Acceptor-Substituted Oligothiophenes. *J. Am. Chem. Soc.* **2012**, *134*, 6052–6056.
45. Demanze, F.; Cornil, J.; Garnier, F.; Horowitz, G.; Valat, P.; Yassar, A.; Lazzaroni, R.; Brédas, J.-L. Tuning of the Electronic and Optical Properties of Oligothiophenes *via* Cyano Substitution: A Joint Experimental and Theoretical Study. *J. Phys. Chem. B* **1997**, *101*, 4553–4558.
46. Baber, A. E.; Jensen, S. C.; Iski, E. V.; Sykes, E. C. H. Extraordinary Atomic Mobility of Au{111} at 80 Kelvin: Effect of Styrene Adsorption. *J. Am. Chem. Soc.* **2006**, *128*, 15384–15385.
47. Gross, L.; Mohn, F.; Moll, N.; Liljeroth, P.; Meyer, G. The Chemical Structure of a Molecule Resolved by Atomic Force Microscopy. *Science* **2009**, *325*, 1110–1114.
48. Mohn, F.; Schuler, B.; Gross, L.; Meyer, G. Different Tips for High-Resolution Atomic Force Microscopy and Scanning Tunneling Microscopy of Single Molecules. *Appl. Phys. Lett.* **2013**, *102*, 073109.
49. Jiang, Y.; Huan, Q.; Fabris, L.; Bazan, G. C.; Ho, W. Submolecular Control, Spectroscopy and Imaging of Bond-Selective Chemistry in Single Functionalized Molecules. *Nat. Chem.* **2013**, *5*, 36–41.
50. Giessibl, F. J. Advances in Atomic Force Microscopy. *Rev. Mod. Phys.* **2003**, *75*, 949–983.
51. Horcas, I.; Fernández, R.; Gómez-Rodríguez, J. M.; Colchero, J.; Gómez-Herrero, J.; Baro, A. M. WSXM: A Software for Scanning Probe Microscopy and a Tool for Nanotechnology. *Rev. Sci. Instrum.* **2007**, *78*, 013705.
52. Ruby, M. SpectraFox Home Page. http://spectrafox.com/.
53. Frisch, M. J.; Trucks, G. W.; Schlegel, H. B.; Scuseria, G. E.; Robb, M. A.; Cheeseman, J. R.; Montgomery, J. A., Jr.; Vreven, T.; Kudin, K. N.; Burant, J. C. *et al. Gaussian 03*, Revision C.02; Gaussian, Inc.: Wallingford, CT, 2004.